Mpho Mendy Nefale[1], *Olumuyiwa Otegbeye*[1*], *Md Sharifuddin Ansari*[2**], *Shina Daniel Oloniiju*[3]

OVERLAPPING MULTI-DOMAIN PAIRED QUASILINEARISATION TECHNIQUE APPLIED TO THE MIXED CONVECTIVE FLOW OF JEFFREY NANOFLUID WITH MICROORGANISM AND ACTIVATION ENERGY

PRIMENA MULTIDOMENSKOG PREKLAPANJA METODOM SPREGNUTE KVAZILINEARIZACIJE NA MEŠOVITI PROTOK KONVEKCIJOM JEFFREY NANOFLUIDA SA MIKROORGANIZMOM I ENERGIJOM AKTIVACIJE

Originalni naučni rad / Original scientific paper
Rad primljen / Paper received: 15.04.2026
https://doi.org/10.69644/ivk-2026-siB-0042

Adresa autora / Author's address:
[1] School of Computer Science and Applied Mathematics, University of the Witwatersrand, Johannesburg, South Africa
M.M. Nefale https://orcid.org/0000-0003-2045-9313 ,
O. Otegbeye https://orcid.org/0000-0003-1321-9776 ;
*email: olumuyiwa.otegbeye@wits.ac.za
[2] School of Technology, Pandit Deendayal Energy University, Gandhinagar 382421, India **email: md.sharifuddin@spt.pdpu.ac.in
Md Sharifuddin Ansari https://orcid.org/0000-0002-9277-0904
[3] Department of Mathematics, Rhodes University, Makhanda, PO Box 94, Grahamstown 6140, South Africa
S.D. Oloniiju https://orcid.org/0000-0002-9794-8580

Keywords

- Jeffrey nanofluid
- bioconvection
- activation energy
- overlapping subdomains
- paired quasilinearisation, spectral method

Abstract

This paper presents an innovative numerical technique, the overlapping multi-domain paired quasilinearisation OMD-PQLM, developed for solving highly nonlinear systems of coupled partial differential equations (PDEs). The OMD-PQLM is based on a strategy in which the equations are paired and treated concurrently, thereby improving computational performance through a reduction in the dimension of the coefficient matrix to be inverted while maintaining the high accuracy associated with spectral-based decoupling methods. The approach entails partitioning the entire computational interval of integration into multiple smaller, overlapping subintervals. Solutions in each subinterval are acquired using boundary conditions and solutions from preceding subdomains. To assess the performance of the proposed technique, an analysis is performed on the governing differential equations. The mathematical model describes a Jeffrey nanofluid characterised by active energy and microorganisms within a mixed convection flow environment. The innovation of the OMD-PQLM provides a new understanding of numerical efficiency by merging overlapping multi-domain techniques with the paired quasilinearisation method (PQLM), which improves solution accuracy and convergence. The findings demonstrate that the OMD-PQLM provides highly accurate results, achieving rapid convergence with errors reaching as low as 10^{-14}. Residual and solution error analyses validate the method's effectiveness and robustness. Flow characteristics concerning controlling parameters are thoroughly analysed, offering valuable insights into the system's physical behaviour, especially the novelty of the model involving motile microorganisms. The study shows that the OMD-PQLM serves as an effective tool for addressing the nonlinear PDEs that often define complex phenomena within engineering research.

Ključne reči

- Jeffrey nanofluid
- biokonvekcija
- energija aktivacije
- preklapanje poddomena
- spregnuta kvazilinearizacija, spektralna metoda

Izvod

U ovom radu je predstavljena inovativna numerička metoda, spregnuta kvazilinearizacija kod multidomenskog preklapanja, OMD-PQLM, razvijena za rešavanje težih nelinearnih sistema spregnutih parcijalnih diferencijalnih jednačina (PDE). OMD-PQLM se zasniva na strategiji gde su jednačine spregnute i tretiraju se istovremeno, čime se poboljšavaju performanse računa smanjenjem dimenzija matrice koeficijenata, koja postaje inverzna, uz održavanje visoke tačnosti spektralnih metoda razdvajanja. Pristup povlači za sobom podelu čitavog računskog intervala integracije u više manjih, preklapajućih podintervala. U svakom podintervalu dobijaju se rešenja korišćenjem graničnih uslova, kao i rešenja iz prethodnih poddomena. Za ocenu performanse predložene metode, izvodi se analiza osnovnih diferencijalnih jednačina. Matematički model opisuje Jeffrey nanofluid, koji karakterišu energija aktivacije i mikroorganizmi unutar mešovite sredine konvektivnog protoka. Inovativnost OMD-PQLM daje novo razumevanje numeričke efikasnosti, integrisanjem metoda preklapanja multi-domena sa spregnutom metodom kvazilinearizacije (PQLM), čime se poboljšava tačnost i konvergencija rešenja. Rezultati pokazuju da OMD-PQLM daje rezultate veće tačnosti, sa brzom konvergencijom, gde se greške smanjuju sve do 10^{-14}. Analize ostataka i greške rešenja potvrđuju efikasnost i robusnost metode. Kontrolni parametri karakteristike protoka su temeljno analizirani, čime se dobijaju korisna saznanja o fizičkom ponašanju sistema, a posebno uvođenje noviteta u modelu, obuhvatanjem specifične pokretljivosti mikroorganizama. Istraživanje pokazuje da je OMD-PQLM efikasan alat za obradu nelinearnih PDE, kojima se često definišu kompleksni fenomeni u oblasti inženjerstva.

INTRODUCTION

A Jeffrey nanofluid is characterised by the suspension of specific nanoparticles within a viscoelastic Jeffrey fluid medium /1/. To characterise fluids displaying both viscous and elastic behaviours, the application of the Jeffrey framework has proven effective, as it accounts for both relaxation and retardation periods, /2/. Consequently, these nanofluids are highly applicable in processes requiring enhanced heat transfer. These nanofluids are used in microelectronic cooling systems, polymer extrusion processes, and biomedical devices that require precise thermal regulation /3-6/. Nadeem et al. /7/ investigated the motion of a Jeffrey nanofluid near a surface extending exponentially. It was reported that an escalation in the ratio between relaxation and retardation periods leads to a thinner velocity boundary layer, characterised by a faster reduction in velocity and a lower local skin-friction coefficient. When forced and free convection interact to enhance heat transfer, the phenomenon is referred to as mixed convection /8/. Recent developments in the field of non-Newtonian nanofluidics have led to a renewed interest in the underlying principles of simultaneous natural and forced convective transport across various fluidic geometries /9-11/. The thermal behaviour of a Jeffrey nanoliquid within channels featuring flexible walls was examined in a recent study /12/. Detailed examination of these dynamics shows that while the thermal profile is enhanced by the effects of Ohmic heating, it is negatively correlated with intensified radiation and Hartmann parameters. A comparable analysis was conducted regarding the magnetohydrodynamic (MHD) transport of Jeffrey-based nanoliquids under mixed-convection conditions, /13/. This investigation reveals that the synergistic effect of intensified magnetic fields and Ohmic heating serve to expand both thermal and hydrodynamic boundary layer thicknesses, which subsequently promotes superior heat transfer efficiency. Further research into the stationary transport of heat and species surrounding an oblique, elongated cylinder reveals that a rise in the Deborah number results in a 20 % enhancement of the axial velocity, /14/. In addition, raising the radiation parameter increases the Nusselt number by almost 39 %, and the coupled influence of double stratification and Joule heating greatly changes the distribution of nanoparticle concentrations /14/. Detailed examination of transport characteristics of a Jeffrey nanoliquid past a horizontally oriented cylinder is conducted under conditions of combined natural and forced convection, /15/. The study utilises the Buongiorno framework to incorporate the mechanisms of thermophoretic drift and Brownian diffusion. In this context, the synergistic influence of chemical responses and thermal radiation on the simultaneous natural and forced convection of a Jeffrey liquid is extensively studied, /16/. This analysis focuses specifically on the flow in the vicinity of an exponentially extending surface. Parallel to this, the MHD transport of a Jeffrey-based nanoliquid within a non-uniform duct is the subject of further investigation, /17/. Under conditions characterised by minimal inertial forces and extended waves, that investigation evaluates the interplay between induced magnetic phenomena, frictional heating, and combined buoyancy effects.

At the end of the nineteenth century, Svante Arrhenius, a Swedish scientist, introduced the concept of activation energy, denoted by the symbol E_a and measured in kilojoules per mole (kJ/mol) /18/. This represents the minimum energy required for molecular or atomic interactions to initiate a chemical reaction. Different reactions exhibit distinct activation energy values, which can sometimes be negligible or even zero. This concept finds applications in fields such as food processing, suspended emulsions, geothermal energy, and chemical engineering. The Buongiorno framework /19/ is utilised to conduct a detailed examination of the transport phenomena within a Jeffrey-based nanoliquid passing over a stretching surface. This study evaluates the interplay between Arrhenius kinetics and frictional heating, while accounting for velocity discontinuity, thermodynamic irreversibility, and the Bejan number. They find that partial slip lowers velocity, while Brownian motion and activation energy raise temperature, concentration, and overall entropy generation. A positive correlation is found between thermodynamic irreversibility and several key physical parameters in the case of a second-grade nanoliquid, /20/. Specifically, the results indicate that the entropy production profile is enhanced by the intensification of inertial forces, viscous heating, magnetic effects, and thermal radiation levels. However, this trend is reversed when considering the temperature-difference parameter, which results in a significant decline. Their work involves the use of the Runge-Kutta-Fehlberg shooting scheme under Arrhenius activation energy to seek numerical solutions. The transient MHD transport of a Jeffrey-based nanoliquid relative to a rapidly mobilised surface is the subject of a recent investigation /21/. This study sought to determine the interplay between Arrhenius kinetics and imposed magnetic phenomena within the system. An analysis is conducted regarding the simultaneous transport of heat and species within a Jeffrey nanoliquid, /22/. The study evaluated the flow in the vicinity of a porous medium featuring exponentially increasing dimensions, while taking into account the mechanisms of an oblique magnetic force and Arrhenius-driven chemical kinetics. Jagadesh et al. /23/ studied a Jeffrey nanofluid in peristaltic motion within a vertically diverging conduit, focusing on flow, mass transfer, and heat processes while accounting for activation energy, internal heat production, radiative heat transfer, and an inclined magnetic field. Their results indicate that mass transfer rates, axial velocity, and concentration are enhanced by the activation energy parameter. Heat and mass transfer rates also increase under specific parameter combinations, offering insights for biomedical and industrial applications. These investigations demonstrate that activation energy plays a significant part in shaping the behaviour of Jeffrey nanofluids, particularly through its influence on velocity, temperature, concentration, and entropy generation under different convective flow conditions.

The phenomenon of bioconvection describes the mechanism by which spontaneous patterns and density stratification are created when motile microorganisms interact with buoyancy-driven effects and suspended nanoparticles. The study of convection induced by motile microorganisms is increasingly gaining attention due to its applications in solar energy collection, wastewater treatment, biological systems, and microfluidic devices such as biomedical dispersions and biogalvanic devices. Additionally, it contributes significantly to the study of microbially enhanced oil recovery, and the formation of hydrocarbon-bearing sedimentary basins. Insufficient mixing presents a significant challenge in various scientific and industrial processes. To address this issue, Kuznetsov /24/ introduces the novel concept of bioconvection in nanofluids through the incorporation of gyrotactic microorganisms. Ansari et al. /25/ investigate bioconvective MHD Casson fluid motion along a nonlinearly stretching surface, taking into consideration non-uniform heat generation, Brownian motion, thermophoresis, and absorption, as well as viscous and Joule dissipation. Their results show that these magnetic and thermal effects substantially modify the flow, heat transfer, and microorganism distribution. Waqas et al. /26/ conduct a dynamic analysis of bioconvection effects involving gyrotactic microorganisms in a Jeffrey nanoliquid along an expanding sheet, taking into account the effect of ferromagnetic nanomaterials and the Lorentz force. Strengthening the ferromagnetic and Lorentz parameters increases heat transfer while decreasing velocity and microorganism density. Algehyne et al. /27/ explore the effect of magnetic and buoyancy forces on the interaction between nanoparticles and microorganisms, taking into account features such as chemical reactions, thermophoresis, Brownian motion, heat absorption and generation, and the Darcy-Forchheimer effect. The results indicate that stronger magnetic, buoyancy, and Darcy-Forchheimer influences decelerated flow, whereas higher heat generation, Eckert, and thermophoretic parameters increase the temperature and nanoparticle concentration. Alqurashi et al. /28/ explore bioconvective transport within the MHD stream of micropolar nanoliquids over a vibrating boundary, considering non-uniform heat sources, motile microorganisms, and melting; they find that enhanced melting raises velocity, micro-rotation, temperature, and microorganism density, while a stronger magnetic field slows the flow yet further increases microorganism density. Alzahrani et al. /29/ perform a study on three-dimensional Jeffrey nanofluid involving motile microorganisms, and it is reported that stronger bioconvection and magnetic fields increase mass and heat transfer but reduce the fluid velocity. To examine the thermal transport characteristics, the research utilises non-Fourier thermal relaxation models alongside fluctuating thermal conductivity and internal energy source/sink mechanisms. The stability of bioconvectional transport driven by gravitactic microorganisms within a non-isotropic porous medium is the subject of a novel study /30/. This investigation utilises the Boussinesq approximation in tandem with a Jeffrey-Darcy framework to examine underlying thermal and biological dynamics. Results show that stronger mechanical anisotropy and a larger Jeffrey number lower the stability threshold for convection, higher Péclet number and microbe concentration intensified instability, while thermal anisotropy is stabilising at low cell density but destabilising at high density. A comprehensive analysis of the bioconvectional transport within a non-Newtonian nanoliquid is conducted in a recent publication /31/. The study focuses on the flow characteristics surrounding an arcuate boundary while integrating the behaviour of motile microorganisms. They find that stronger magnetic fields diminish the velocity boundary layer but raise temperature and nanoparticle concentration. A numerical exploration into the bioconvective transport of a tangent hyperbolic nanoliquid is conducted /32/. This investigation focuses on the flow passing over a porous surface characterised by exponential expansion, subject to specific interfacial conditions while incorporating the effects of an applied magnetic force alongside the motility of microorganisms. The study incorporates key factors such as activation energy, radiative heat transfer, Ohmic heating, and a spatially varying internal heat source. It is reported that higher magnetic and Weissenberg numbers reduce the velocity field, mixed-convection and radiation parameters enhance heat transfer, and larger bioconvection Lewis and microorganism slip numbers decrease microorganism density.

Developing efficient numerical algorithms to solve these highly nonlinear coupled differential systems and other equally demanding engineering problems remains a central research priority in computational mathematics. Spectral methods, renowned for their high accuracy and exponential convergence rates, have been extensively employed to tackle complex problems in disciplines such as fluid dynamics, heat transfer, and boundary layer flows /33-35/. Techniques based on spectral discretisation and iterative linearisation have proven effective in various applications, /36-39/. However, these methods often encounter challenges when dealing with large computational domains or require enhancements in computational efficiency, /40/.

To overcome limitations of traditional spectral methods, domain decomposition techniques have been introduced, partitioning the computational domain into smaller subdomains to enhance efficiency and accuracy /41/. Numerical strategies based on quasilinearisation within partitioned spectral domains have conclusively been shown to optimise computational precision. Specifically, overlapping and bivariate iterations of this type have been found to significantly improve the speed of convergence /42-43/. In this study, we propose a novel numerical algorithm called the overlapping multi-domain paired quasilinearisation (OMD-PQLM). A variant of the OMD-PQLM is applied to solve the MHD Williamson-nanofluid motion across an exponentially extending sheet modelled by a strong nonlinear set of ordinary differential equations (ODEs), demonstrating higher accuracy than standard paired quasilinearisation (PQLM) /44/. The OMD-PQLM works by pairing equations and solving them simultaneously. The method divides the entire computational domain into several smaller, overlapping subdomains. This implementation of overlapping enhances solution convergence and overall accuracy. Previous studies have addressed similar problems using different numerical techniques. For instance, Khan and Tlili /45/ utilise a homotopic algorithm to examine Jeffrey nanofluid motion in a gyrotactic microorganism environment, thereby demonstrating the influence of the primary system variables on the resulting flow characteristics. While their method demonstrates effectiveness, its accuracy heavily depends on careful parameter selection, which can be a limitation in complex applications.

The current investigation utilises the OMD-PQLM framework to evaluate the triple convective transport of a Jeffrey-type nanoliquid. This model characterises the dynamics in the proximity of a suddenly mobilised interface, incorporating the influence of activation energy and microorganisms. This problem is significant in engineering and biological applications, where accurate modelling of fluid flow with chemical reactions and microbial interactions is crucial. OMD-PQLM demonstrates highly accurate results, with convergence and accuracy validated through residual and solution error analysis. Flow characteristics are thoroughly analysed concerning relevant controlling parameters, showcasing the method's robustness and effectiveness in overcoming the limitations of existing numerical techniques.

MATHEMATICAL REPRESENTATION OF THE PHYSICAL SYSTEM

Free convection flow of Jeffrey nanofluid along with motile microorganisms is studied. For $t > 0$, the boundary surface remains stationary, and the fluid's temperature, nanoparticle content, and microbe density are all prescribed as zero. When $t > 0$, the bounding surface starts moving with uniform velocity q_s along x, i.e., the vertically upward direction, and fluid temperature, microorganism density, and concentration of nanoparticles at the plate are maintained at T_s, C_s, and N_s, whereas the free stream values of those are T_∞, C_∞, and N_∞. The heat-transfer study accounts for the joint influence of bioconvection, viscous dissipation, thermophoresis, and Brownian diffusion together with activation energy. Imposing the initial and boundary constraints in Eq.(5) alongside the non-dimensional governing relations in Eqs.(1)-(4) reproduces the flow model.

$$\frac{\partial^2\omega}{\partial y^2}+\lambda_2\left(\frac{\partial^3\omega}{\partial t\partial y^2}\right)-(1+\lambda_1)\frac{\partial\omega}{\partial t}-(1+\lambda_1)M\omega(1+\lambda_1)\Delta+ +(\theta-Q_1\phi-Q_2h)=0\,, \tag{1}$$

$$\frac{1}{\Pr}\frac{\partial^2\theta}{\partial y^2}-\frac{\partial\theta}{\partial t}+\mathrm{Nb}\frac{\partial\phi}{\partial y}\frac{\partial\theta}{\partial y}+N_\theta\left(\frac{\partial\theta}{\partial y}\right)^2+\frac{\mathrm{Ec}}{1+\lambda_1}\left\{\left(\frac{\partial\omega}{\partial y}\right)^2+ +\lambda_2\frac{\partial\omega}{\partial y}\frac{\partial^2\omega}{\partial t\partial y}\right\}=0\,, \tag{2}$$

$$\frac{\partial^2\phi}{\partial y^2}-\mathrm{Le}\frac{\partial\phi}{\partial t}+\mathrm{Le}K(1+\delta\theta)^n\exp\left(-\frac{E}{1+\delta\theta}\right)\phi+\frac{N_\theta}{N_b}\frac{\partial^2\theta}{\partial y^2}=0\,, \tag{3}$$

$$\frac{\partial^2 h}{\partial y^2}-\mathrm{lb}\frac{\partial h}{\partial t}+\mathrm{Pe}(\delta_1+h)\frac{\partial^2\phi}{\partial y^2}-\mathrm{Pe}\frac{\partial h}{\partial y}\frac{\partial\phi}{\partial y}=0\,, \tag{4}$$

where: ω, θ, ϕ, and h are respectively, dimensionless fluid velocity, fluid temperature, nanoparticle concentration, and microorganism density.

Mathematically, the flow problem is constrained by the following initial and boundary conditions:

- initial conditions

$\omega(y, 0) = 0,\ \theta(y, 0) = 0,\ \phi(y, 0) = 0,\ h(y, 0) = 0,\ t = 0,\ y > 0,$

- boundary conditions at the surface

$\omega(0, t) = 1,\ \theta(0, t) = 1,\ \phi(0, t) = 1,\ h(0, t) = 1,\ t > 0, y = 0,$

- and boundary conditions in the far field

$$\omega(y,t) \to 0,\ \theta(y,t) \to 0,\ \phi(y,t) \to 0,\ h(y,t) \to 0,\ t > 0, y \to \infty, \tag{5}$$

where:

$$M=\frac{\sigma B^2\nu}{\rho w_0^2},\ \Pr=\frac{\nu}{\alpha},\ \lambda=\frac{\lambda_2 w_0^2}{\nu},\ \delta=\frac{\theta_w-\theta_\infty}{\theta_\infty},$$
$$N_b=\frac{\tau D_B(\phi_w-\phi_\infty)}{\nu},\ N_t=\frac{\tau D_\theta(\theta_w-\theta_\infty)}{\nu\theta_w},\ k=\frac{k_r^2\nu}{w_0^2},$$
$$\mathrm{Le}=\frac{\nu}{D_B},\ \alpha=\frac{k}{\rho c_f},\ \mathrm{Ec}=\frac{w_0^2}{c_f(\theta_w-\theta_\infty)},\ E=\frac{E_a}{k\theta_\infty}\,. \tag{6}$$

The physical parameters considered in this work, namely the skin friction coefficient C_{fx}, the Nusselt number Nu_x, the Sherwood number Sh_x, and N_{mx}, which represents the local motile microorganism concentration, are defined as

$$C_{fx}=\frac{\mu}{1+\lambda_1}\left(1+\lambda_2\frac{\partial}{\partial t}\right)\frac{\partial\omega}{\partial y}\bigg|_{y=0},\quad \mathrm{Nu}_x=-\frac{\partial\theta}{\partial y}\bigg|_{y=0},$$
$$\mathrm{Sh}_x=-\frac{\partial\phi}{\partial y}\bigg|_{y=0},\quad N_{mx}=-\frac{\partial h}{\partial y}\bigg|_{y=0}.$$

Below, the list of includes variables and measures involved.

lb		bioconvection Lewis number
n		fitted rate constant
λ_1		proportion of relaxation to retardation time
K		chemical reaction parameter
δ_1	$n_\infty/(n_s-n_\infty)$	bioconvection parameter
δ	$(T_s-T_\infty)/T_\infty$	temperature difference
E	E_a/kT_∞	Arrhenius activ. energy parameter
Δ	$\mathrm{Gr}_x/\mathrm{Re}_x^2$	Richardson number
Q_1		buoyancy ratio parameter
Pr	ν/α	Prandtl number
M	$\sigma B^2\nu/\rho q_s^2$	magnetic parameter
N_b	$\tau D_B(\phi_s-\phi_\infty)/\nu$	Brownian motion parameter
Pe		Peclet number
Le		Lewis number
N_θ	$\tau D_T(T_s-T_\infty)/\nu T_\infty$	thermophoresis parameter
Ec	$q_s^2/\nu(T_s-T_\infty)$	Eckert number
Gr_x	$((1-\phi_\infty)/\nu^2)x^3g\beta(T_s-T_\infty)$	Grashof number
Re_x	$(q_sx)/\nu$	Reynold number
Q_2		bioconvection Rayleigh number

FORMULATION OF THE OMD PQLM

The following section provides an overview of the OMD-PQLM structure in relation to a broad collection of partial differential equations (PDEs) consisting of K coupled equations with K dependent variables. We define the governing PDE system as follows:

$$\mathscr{F}_j[\omega_1(\xi,\tau),\omega_2(\xi,\tau),\ldots,\omega_K(\xi,\tau)]=0,\ \ j=1,2,\ldots,K. \tag{7}$$

Equation (7) represents a coupled, nonlinear PDE system, where $\mathscr{F}_j$ denotes the j-th nonlinear operator for $j = 1, \ldots, K$. The solution set $\{\omega_1, \omega_2, \ldots, \omega_K\}$ is defined by the collection: $[\{\omega_1^{(0)}, \omega_1^{(1)}, \ldots, \omega_1^{(r1)}\}, \ldots, \{\omega_K^{(0)}, \omega_K^{(1)}, \ldots, \omega_K^{(r1)}\}]$.

Paired quasilinearisation method

To address Eq.(7), we utilise the PQLM, /39/. While pairings can technically be assigned stochastically, we adopt a sequential ordering to clarify the PQLM implementation. Assuming $\{w_1, w_2\}$ constitutes the primary pair, the quasilinearisation is applied to operators $\mathscr{F}_1(w_1, \ldots, w_K)$ and $\mathscr{F}_2(w_1, \ldots, w_K)$ to yield a linearised system. This iterative procedure is subsequently applied to consecutive pairs, where the refined solutions from previous pairings are used to update the succeeding ones. The pairing structure is generalised as:

$$\mathscr{F}_b[w_1, \ldots, w_K] = 0,\ b \in \{\{1,2\}, \{3,4\}, \ldots, \{K-1, K\}\}. \quad (8)$$

Overlapping computational domains

The overlapping strategy is implemented across both spatial and temporal dimensions. The total spatial integration interval $[\xi_0, \xi_f]$ is partitioned into S overlapping subdomains, each of length Δ_ξ, denoted as:

$$\mathscr{A}_p = [\xi_0{}^p, \xi_{N\xi}{}^p],\quad p = 1, 2, \ldots, S\,. \quad (9)$$

Each segment is subdivided using a set of $N_\xi + 1$ collocation points. Similarly, the temporal domain $[\tau_0, \tau_f]$ is divided into T overlapping subdomains of length Δ_τ, defined by:

$$\mathscr{B}_q = [\tau_0{}^q, \tau_{N\tau}{}^q],\quad q = 1, 2, \ldots, T\,. \quad (10)$$

Within the $\mathscr{A}_p$ and $\mathscr{B}_q$ subintervals, the final two nodes overlap with the first two nodes of the subsequent intervals $\mathscr{A}_{p+1}$ and $\mathscr{B}_{q+1}$, respectively. These subinterval lengths are rigorously defined as:

$$\Delta_\xi = \frac{\xi_f - \xi_0}{S + \frac{1}{2}(1-S)\left(1-\cos\left(\frac{\pi}{N_\xi}\right)\right)}, \quad (11)$$

$$\Delta_\tau = \frac{\tau_f - \tau_0}{T + \frac{1}{2}(1-T)\left(1-\cos\left(\frac{\pi}{N_\tau}\right)\right)}. \quad (12)$$

Here, $N_\xi + 1$ and $N_\tau + 1$ represent the density of collocation points in their respective intervals. The total spatial interval can be expressed as:

$$\xi_f - \xi_0 = 2\Delta_\xi - \delta + (2\Delta_\xi - 2\delta)\left(\frac{s}{2} - 1\right) = 2\Delta_\xi - \delta + (\Delta_\xi - \delta)(S-2) \quad (13)$$

Equation (13) serves as the basis for deriving Eq.(11), where δ signifies the overlapping distance.

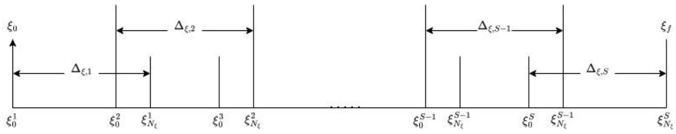

Figure 1. The spatial domain configuration featuring an overlapping grid.

Figure 1 illustrates the overlapping grid structure for the spatial interval; a mirrored configuration is applied to the temporal domain. We define $\delta = \xi_0 - \xi_1$, focusing on the primary interval $\mathscr{A}_1$, where $\xi \in [\xi_0, \xi_{N\xi}{}^1]$ and the length is $\Delta_\xi = \xi_{N\xi}{}^1 - \xi_0$, we apply a linear mapping $\xi = \frac{\Delta_\xi}{2}\eta + \frac{\xi_0 + \xi^1_{N_\xi}}{2}$ to convert the domain into the spectral domain $[-1, 1]$. Utilising Gauss-Lobatto nodes $\eta_m = \cos(\pi m/N_\xi)$ for $m = 0,1, \ldots, N_\xi$, we find:

$$\delta = \xi_0 - \xi_1 = \frac{\Delta_\xi}{2}(\eta_0 - \eta_1) = \frac{\Delta_\xi}{2}\left(1-\cos\left(\frac{\pi}{N_\xi}\right)\right). \quad (14)$$

Consequently, the total length in Eq.(13) becomes:

$$\xi_f - \xi_0 = \delta(1-S) + S\Delta_\xi = \frac{\Delta_\xi}{2}\left(1-\cos\left(\frac{\pi}{N_\xi}\right)\right)(1-S) + S\Delta_\xi\,. \quad (15)$$

Solving for Δ_ξ recovers Eq.(13). A similar derivation provides the temporal interval length.

Preceding the application of the spectral collocation method within every discrete subinterval, the intervals $\mathscr{A}_p$ and $\mathscr{B}_q$ are mapped to $\eta \in [-1, 1]$ and $\sigma \in [-1, 1]$ via:

$$\xi_m^p = \frac{\xi^p_{N_\xi} - \xi^p_0}{2}\eta + \frac{\xi^p_{N_\xi} + \xi^p_0}{2},\quad \{\eta_m\}_{m=0}^{N_\xi} = \cos\left(\frac{\pi m}{N_\xi}\right), \quad (16)$$

$$\tau_n^q = \frac{\tau^q_{N_\tau} - \tau^p_0}{2}\sigma + \frac{\tau^q_{N_\tau} + \tau^q_0}{2},\quad \{\sigma_n\}_{n=0}^{N_\tau} = \cos\left(\frac{\pi n}{N_\tau}\right). \quad (17)$$

Spectral discretisation technique

This segment illustrates the use of the Chebyshev spectral collocation technique to resolve the governing equations represented by Eqs.(1)-(4) in both spatial and temporal dimensions /46/. As established previously, the overlapping computational domains $\mathscr{A}_p$ and $\mathscr{B}_q$ undergo linear mapping into the canonical coordinates $\eta \in [-1, 1]$ and $\sigma \in [-1, 1]$, respectively. The computational procedure for evaluating the local solutions $w_{1,r}(\eta, \sigma), \ldots, w_{K,r}(\eta, \sigma)$ involves the utilisation of bivariate Lagrange interpolants, structured as:

$$w_1(\eta,\sigma) \approx \sum_{i=0}^{N_\xi}\sum_{j=0}^{N_\tau} w_1(\eta_i,\sigma_j)\phi_i(\eta)\psi_j(\sigma)\,,$$

$$w_2(\eta,\sigma) \approx \sum_{i=0}^{N_\xi}\sum_{j=0}^{N_\tau} w_2(\eta_i,\sigma_j)\phi_i(\eta)\psi_j(\sigma)\,,$$

$$\vdots\,,$$

$$w_K(\eta,\sigma) \approx \sum_{i=0}^{N_\xi}\sum_{j=0}^{N_\tau} w_K(\eta_i,\sigma_j)\phi_i(\eta)\psi_j(\sigma)\,, \quad (18)$$

where: ϕ_i and ψ_j represent cardinal basis functions defined by the products:

$$\phi_i(\eta) = \prod_{l=0,l\neq i}^{N_\xi} \frac{\eta - \eta_l}{\eta_i - \eta_l}\,,$$

$$\psi_j(\sigma) = \prod_{k=0,k\neq j}^{N_\tau} \frac{\sigma - \sigma_k}{\sigma_j - \sigma_k}\,, \quad (19)$$

which satisfy the Kronecker delta property at nodal points:

$$\phi_i(\eta_l) = \delta_{i,l} = \begin{cases} 0 & \text{if } i \neq l \\ 1 & \text{if } i = l \end{cases},$$

$$\psi_j(\sigma_k) = \delta_{j,k} = \begin{cases} 0 & \text{if } i \neq l \\ 1 & \text{if } i = l \end{cases}. \quad (20)$$

The discretisation utilises the Chebyshev-Gauss-Lobatto nodes, denoted by η_i and σ_j, consistent with the definitions in Eqs.(21) and (22):

$$\eta_i = \cos\left(\frac{\pi i}{N_\xi}\right),\quad i = 0,1,\ldots,N_\xi\,, \quad (21)$$

$$\sigma_j = \cos\left(\frac{\pi j}{N_\tau}\right),\quad j = 0,1,\ldots,N_\tau\,. \quad (22)$$

The differentiation operators D_η and D_σ are derived by scaling the canonical differentiation matrices to reflect the physical dimensions of the subdomains /46/. These transformed matrices are explicitly given by:

$$D_\xi = \frac{2}{\Delta_\xi}D_\eta \quad (23)$$

$$D_\tau = \frac{2}{\Delta_\tau}D_\sigma\,, \quad (24)$$

with respect to the spatial and temporal coordinates, in respect, we can approximate the partial derivatives of the state variables by employing these operational matrices.

COMPUTATIONAL STRATEGY FOR SYSTEM APPROXIMATION

This segment outlines the application of OMD PQLM. The approximations involve the pairing of $\{\omega, \theta\}$ and $\{\phi, h\}$. Nonlinear terms are approximated by the application of the first order Taylor series, as a result

$$[a_0]\omega''_{r+1}+[a_1]\omega_{r+1}+[a_2]\frac{\partial\omega''_{r+1}}{\partial t}+[a_3]\frac{\partial\omega_{r+1}}{\partial t}+[a_4]\theta_{r+1}=a_5 \quad (25)$$

$$[b_0]\omega'_{r+1}+[b_1]\frac{\partial\omega'_{r+1}}{\partial t}+[b_2]\theta''_{r+1}+[b_3]\theta'_{r+1}+[b_4]\frac{\partial\theta_{r+1}}{\partial t}=b_5 \quad (26)$$

where: a_0 1; $a_1 = -(1+\lambda_1)M$; $a_2 = \lambda_2$; $a_3 = -(1+\lambda_1)$; $a_4 = (1+\lambda_1)$; $a_5 = -(1+\lambda_1)\Delta(-Q_1\phi_r - Q_2h_r)$;

$$b_0=\frac{\mathrm{Ec}}{1+\lambda_1}\left(2\omega'_r+\lambda_2\frac{\partial\omega'_r}{\partial t}\right);\ b_1=\frac{\mathrm{Ec}\,\lambda_2}{1+\lambda_1}\omega'_r;\ b_2=\frac{1}{\mathrm{Pr}};$$

$$b_3=N_b\phi'_r+2N_\theta\theta'_r;\ b_4=-1;$$

$$b_5=N_\theta\theta_r'^2+\frac{\mathrm{Ec}}{1+\lambda_1}\left(\omega_r'^2+\lambda_2\omega'_r\frac{\partial\omega'_r}{\partial t}\right). \quad (27)$$

The most recent iterations for f and θ are utilised in the subsequent couple of equations,

$$[c_0]\phi''_{r+1}+[c_1]\phi_{r+1}+[c_2]\frac{\partial\phi_{r+1}}{\partial t}=c_3, \quad (28)$$

$$[e_0]\phi''_{r+1}+[e_1]\phi'_{r+1}+[e_2]h''_{r+1}+[e_3]h'_{r+1}+[e_4]h_{r+1}+ +[e_5]\frac{\partial h_{r+1}}{\partial t}=e_6, \quad (29)$$

where: $c_0 = 1$; $c_1 = -\mathrm{Le}K(1+\delta\theta_{r+1})^n e^{-E/(1+\delta\theta_{r+1})}$; $c_2 = -\mathrm{Le}$; $c_3=-\frac{N_\theta}{N_b}\theta''_{r+1}$; $e_0 = -\mathrm{Pe}(\delta_1 + h_r)$; $e_1 = -\mathrm{Pe}h_r'$; $e_2 = 1$; $e_3 = -\mathrm{Pe}\phi_r'$; $e_4 = -\mathrm{Pe}\phi_r''$; $e_5 = -\mathrm{lb}$; $e_6 = -\mathrm{Pe}h_r\phi_r'' - \mathrm{Pe}h_r'\phi_r'$.

Through the application of the Chebyshev spectral collocation approach and the subdomain strategy, the decoupled linearised equation pairs are computed in the following manner:

$$\left([a_0]D_\xi^2+[a_1]\right)\Omega_{r+1}+[a_2]\sum_{n=0}^{M_t-1}d_{\tau,mn}D_\xi^2\Omega_{r+1,n}+ +[a_3]\sum_{n=0}^{M_t-1}d_{\tau,mn}\Omega_{r+1,n}+[a_4]\Theta_{r+1}=R_{1,m}, \quad (31)$$

$$[b_0]D_\xi\Omega_{r+1}+[b_1]\sum_{n=0}^{M_t-1}d_{\tau,mn}D_\xi\Omega_{r+1,n}+\left([b_2]D_\xi^2+ +[b_3]D_\xi\right)\Theta_{r+1}+[b_4]\sum_{n=0}^{M_t-1}d_{\tau,mn}\Theta_{r+1,n}=R_{2,m}, \quad (32)$$

$$\left([c_0]D_\xi^2+[c_1]I\right)\Phi_{r+1}+[c_2]\sum_{n=0}^{M_t-1}d_{\tau,mn}\Phi_{r+1,n}=R_{3,m}, \quad (33)$$

$$\left([e_0]D_\xi^2+[e_1]D_\xi\right)\Phi_{r+1}+\left([e_2]D_\xi^2+[e_3]D_\xi+[e_4]I\right)H_{r+1}+ +[e_5]\sum_{n=0}^{M_t-1}d_{\tau,mn}H_{r+1,n}=R_{4,m}, \quad (34)$$

where:

$$R_{1,n}=-\lambda_2\frac{\partial\omega''_r}{\partial t}+(1+\lambda_1)\frac{\partial\omega_r}{\partial t}+a_5, \quad (35)$$

$$R_{2,n}=\frac{\partial\theta}{\partial t}-\frac{\mathrm{Ec}}{1+\lambda_1}\left(\lambda_2\omega'_r\frac{\partial\omega'_r}{\partial t}\right)+b_5, \quad (36)$$

$$R_{3,n}=\mathrm{Le}\frac{\partial\phi}{\partial t}+c_3, \quad (37)$$

$$R_{4,n}=\mathrm{lb}\frac{\partial h}{\partial t}+e_6. \quad (38)$$

RESULTS AND ANALYSIS

Using OMD-PQLM, we compute the solutions for the system in Eqs.(1)-(4) associated with boundary constraints specified in Eq.(5). The OMD-PQLM utilises $N_\xi = 5$ and N_τ grid points, with $S = 8$ and $T = 6$ subintervals for spatial and temporal domains, respectively. The count of overlapping domains is increased to increase the method's accuracy. To monitor convergence, successive iterates are compared and their difference is measured with the infinity norm:

$$E^{(r+1)}=\left\|u^{(r+1)}-u^r\right\|_\infty,$$

where: $E^{(r+1)}$ is the solution error after iteration $(r + 1)$.

Solution errors from subsequent iterations, along with the infinity norms of these errors, are presented in Figs. 2 to 5. OMD-PQLM demonstrates rapid convergence, achieving convergence in fewer than 9 iterations for all ω, θ, ϕ and h. All solutions converge to a high degree of accuracy, with errors reaching as low as 10^{-13} to 10^{-14} This indicates the method's efficiency and robustness in handling complex non-linear equations. The swift convergence is attributed to the effective combination of the overlapping multidomain approach and the paired quasilinearisation method, which collectively enhance computational efficiency and accuracy.

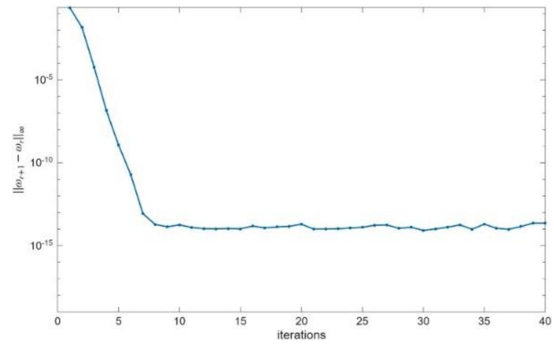

Figure 2. Variation in ω between subsequent iterations.

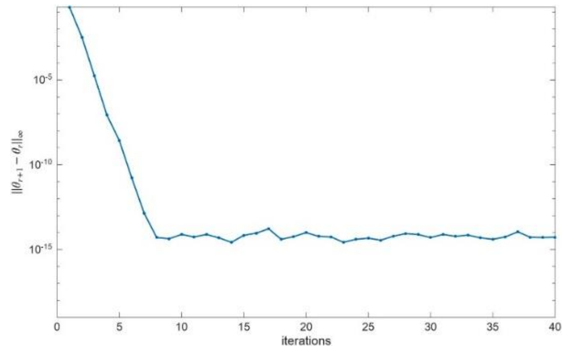

Figure 3. Variation in θ between subsequent iterations.

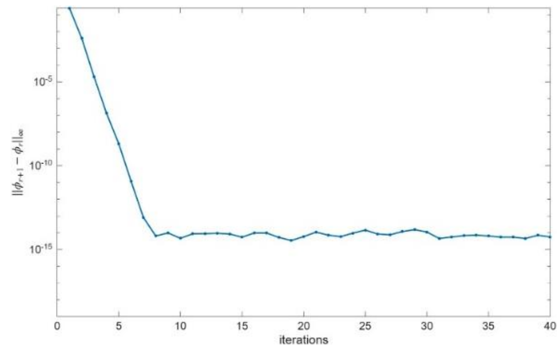

Figure 4. Variation in ϕ between subsequent iterations.

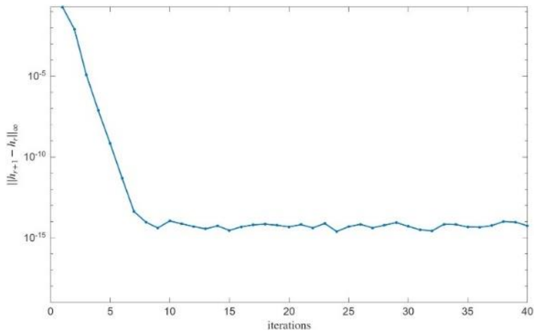

Figure 5. Variation in *h* between subsequent iterations.

Resulting approximate outcomes generated by the OMD-PQLM approach must be subsequently inserted within the converted governing formulations to evaluate residual norms using the following procedure:

$$\left\|\mathrm{Res}(\Omega)\right\|_{\infty}=\left\|\left(\frac{\partial^2\omega}{\partial y^2}+\lambda_2\left(\frac{\partial^3\omega}{\partial t\partial y^2}\right)-(1+\lambda_1)\frac{\partial\omega}{\partial t}-(1+\lambda_1)M\omega+\right.\right.$$
$$\left.\left.+(1+\lambda_1)\Delta(\theta-Q_1\phi-Q_2h)\right)\right\|_{\infty}, \tag{39}$$

$$\left\|\mathrm{Res}(\Theta)\right\|_{\infty}=\left\|\left(\frac{1}{\mathrm{Pr}}\frac{\partial^2\theta}{\partial y^2}-\frac{\partial\theta}{\partial t}+N_b\frac{\partial\phi}{\partial y}\frac{\partial\theta}{\partial y}+N_\theta\left(\frac{\partial\theta}{\partial y}\right)^2+\right.\right.$$
$$\left.\left.+\frac{\mathrm{Ec}}{1+\lambda_1}\left\{\left(\frac{\partial\omega}{\partial y}\right)^2+\lambda_2\frac{\partial\omega}{\partial y}\frac{\partial^2\omega}{\partial t\partial y}\right\}\right)\right\|_{\infty}, \tag{40}$$

$$\left\|\mathrm{Res}(\Phi)\right\|_{\infty}=\left\|\left(\frac{\partial^2\phi}{\partial y^2}-\mathrm{Le}\frac{\partial\theta}{\partial t}-\mathrm{Le}\,K(1+\delta\theta)^n\exp\left(-\frac{E}{1+\delta\theta}\right)\phi+\right.\right.$$
$$\left.\left.+\frac{N_\theta}{N_b}\frac{\partial^2\theta}{\partial y^2}\right)\right\|_{\infty}, \tag{41}$$

$$\left\|\mathrm{Res}(H)\right\|_{\infty}=\left\|\left(\frac{\partial^2 h}{\partial y^2}-\mathrm{lb}\frac{\partial h}{\partial t}-\mathrm{Pe}(\delta_1+h)\frac{\partial^2\phi}{\partial y^2}-\mathrm{Pe}\frac{\partial h}{\partial y}\frac{\partial\phi}{\partial y}\right)\right\|_{\infty}. \tag{42}$$

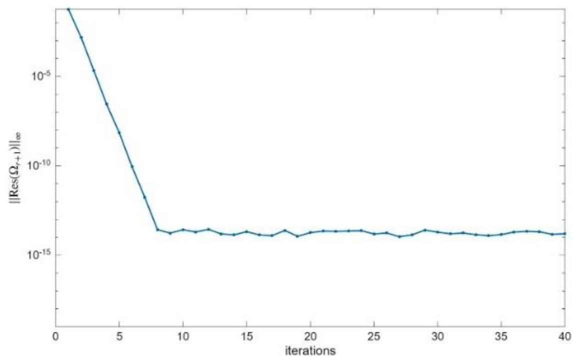

Figure 6. Iterations vs. $\|\mathrm{Res}(\Omega_{r+1})\|_{\infty}$.

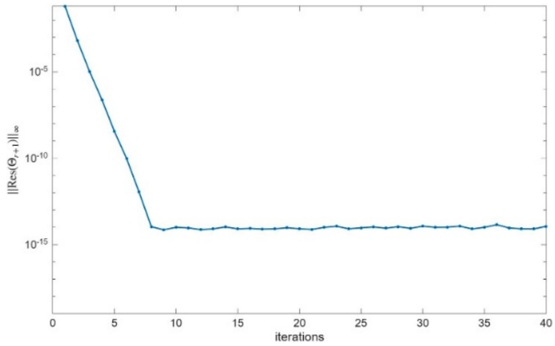

Figure 7. Iterations vs. $\|\mathrm{Res}(\theta_{r+1})\|_{\infty}$.

Figures 6 to 9 display the residual errors obtained using the OMD-PQLM against the iterations count. The residual error is crucial for evaluating accuracy by assessing how closely the estimated solution satisfies the governing equations. It is evident that with an increase in iteration count, there is a decrease in residual errors, indicating an improvement in accuracy. The OMD-PQLM achieves residual errors as low as 10^{-14}, showcasing its effectiveness as an accurate technique for tackling the system of equations.

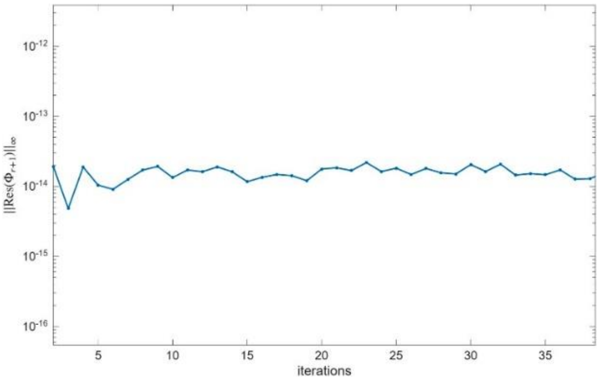

Figure 8. Iterations vs. $\|\mathrm{Res}(\phi_{r+1})\|_{\infty}$.

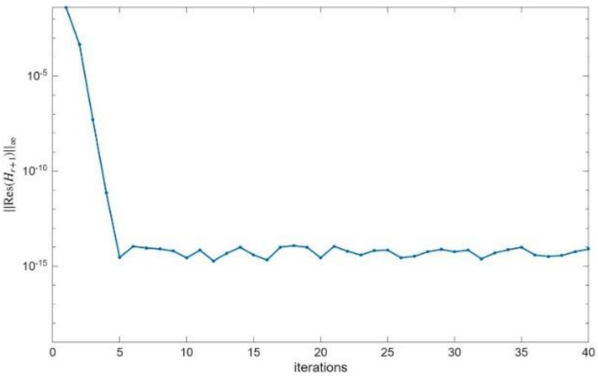

Figure 9. Iterations vs. $\|\mathrm{Res}(H_{r+1})\|_{\infty}$.

The influence of the buoyancy parameter, Q_1

Buoyancy parameter Q_1 is associated with a reduction in the hydrodynamic boundary layer; the profiles of velocity ω slow down near the boundary surface. This phenomenon can be characterised as a stronger influence of buoyancy forces counteracting flow momentum. These effects are captured in Fig. 10.

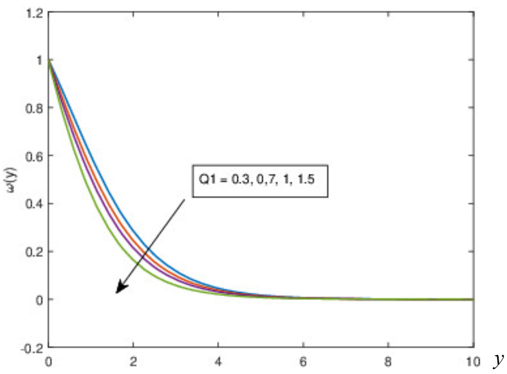

Figure 10. Role of Q_1 on ω.

Role of the bioconvection Rayleigh number, Q_2

A ratio of buoyancy force due to the swimming of microorganisms to viscous force is termed the bioconvection Rayleigh number. A stronger bioconvection number conveys a stronger buoyancy force caused by microorganism distribution, i.e., a development in microorganism concentration gradients causing upward or downward movement in fluid regions, which results in a reduction in fluid motion. This fact is captured in Fig. 11.

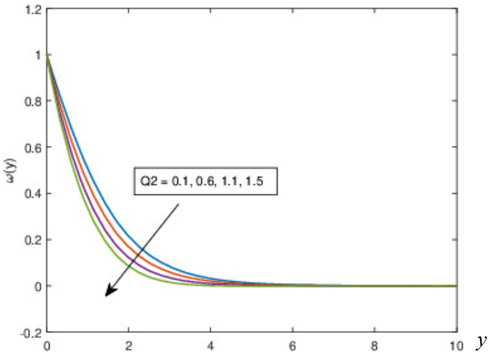

Figure 11. Role of Q_2 on ω.

The influence of the temperature difference, δ

An increment in temperature difference δ implies a larger temperature difference between the boundary and ambient temperature. More width in this difference causes nanoparticles to flow from hot to cool regions. This phenomenon is captured in Fig. 12. Nanoparticle concentration boundary layers become thinner.

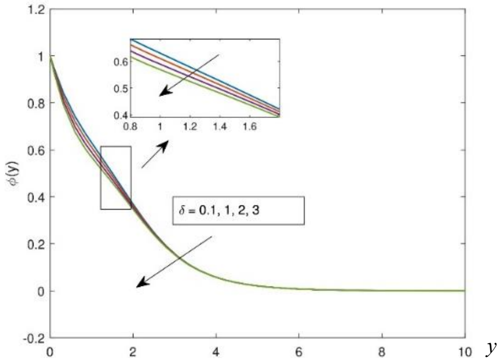

Figure 12. Role of δ on ϕ.

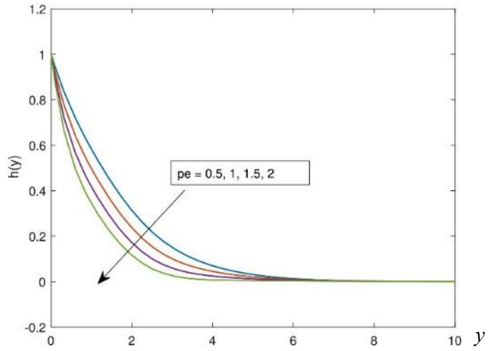

Figure 13. *Role* of Pe on h.

Role of the Peclet number, Pe

Effects of Peclet number Pe on microorganism density are illustrated in Fig. 13. The Peclet number performs a comparison between the rate of advection and the rate of diffusion. Higher values of Peclet number point to a good domination of advection over diffusion; hence, this obstructs the emergence of dense microorganism layers, resulting in a marked decline in microorganism concentration within the boundary-layer region.

The influence of the bioconvection Lewis number, lb

A sketch of the consequences of bioconvection Lewis number lb on microorganism density is presented in Fig. 14. Bioconvection Lewis number tails off with the density of microorganisms close to the boundary. A slower diffusion of microorganisms occurs in comparison with heat transfer in fluid for higher values of lb. This slower diffusion of microorganisms results in a deterioration in their density.

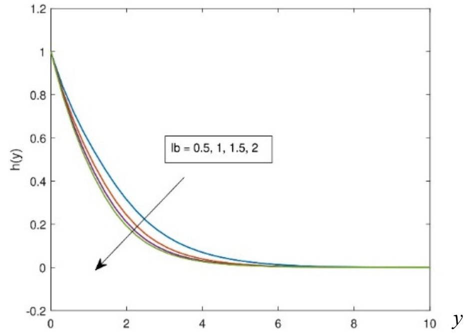

Figure 14. Role of lb on h.

Behaviour of the solutions associated with the chemical reaction parameter, K

Parameter K is directly proportional to the chemical reaction rate. A higher value of K means a faster chemical reaction rate. This parameter shows a significant effect in the bioconvection buoyancy-driven flow system. As the rate of chemical reaction goes up, the nanoparticle concentration and density of microorganisms both decline. This attribute is visualised in Figs. 15 and 16.

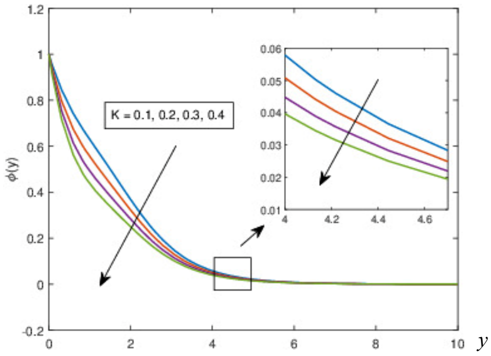

Figure 15. Role of K on ϕ.

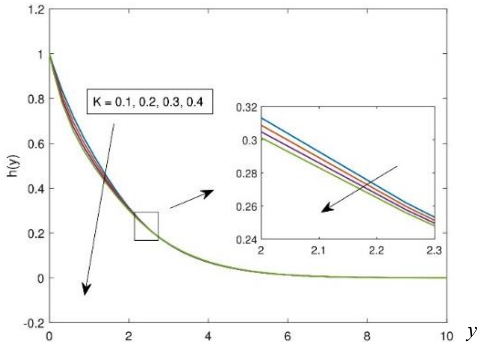

Figure 16. The role of K on h.

The influence of relaxation-retardation time ratio, λ_1

Variations of λ_1 reflect the material's elastic and viscous response. Higher and lower ratios correspond to more viscous and elastic behaviour, that is, slower and faster recovery, in respect. As λ_1 increases, indicating a larger ratio of relaxation time to retardation time results in increased viscosity of the fluid, leading to a decrease in velocity ω within the fluid boundary layer.

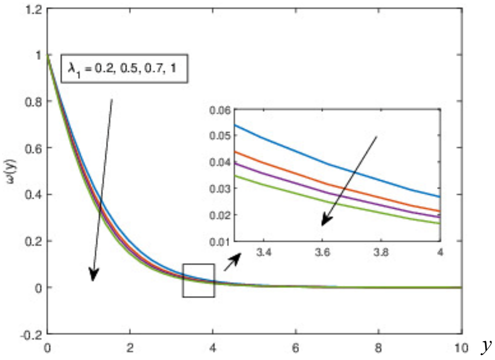

Figure 17. The role of λ_1 on ω.

Role of the Prandtl number, Pr

Figures 18-21 indicate that increasing the Prandtl number Pr leads to lower ω and θ profiles, a higher h profile, and a complex behaviour in ϕ, which decreases initially and then increases beyond a certain point. The reductions in ω and θ suggest that higher Pr values, corresponding to lower thermal diffusivity, slow down the fluid flow and heat transfer. The increase in h implies that the motile microorganism density is enhanced, possibly due to altered thermal conditions favouring their activity. The behaviour of ϕ reflects a nuanced interaction between thermal and mass diffusion processes at different distances from the wall.

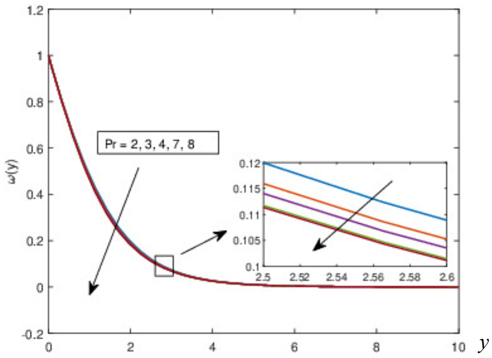

Figure 18. Role of Pr on ω.

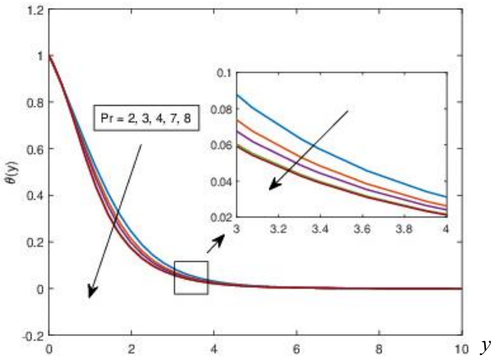

Figure 19. Role of Pr on θ.

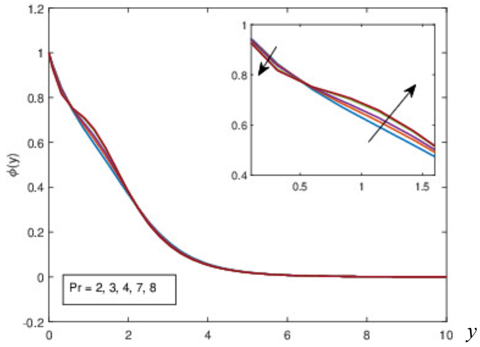

Figure 20. The role of Pr on ϕ.

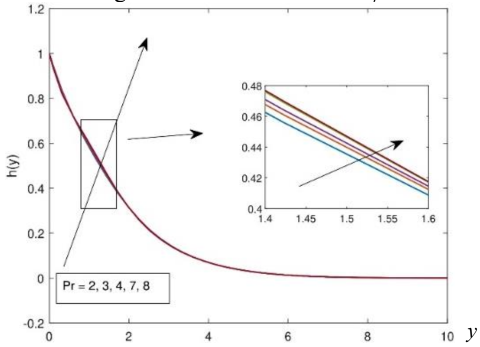

Figure 21. Role of Pr on h.

Role of the magnetic parameter, M

A substantial rise in magnetic parameter M results in a decline in ω and h and rise in θ and ϕ, as depicted in Figs. 22-25. The decline in ω suggests that the applied magnetism exerts a Lorentz force opposing the fluid motion, effectively damping the flow. The increase in ω and ϕ implies that the suppression of convection leads to higher temperatures and nanoparticle concentrations near the wall. The decrease in h may be due to the magnetic field's influence on the microorganisms, potentially hindering their mobility or affecting their distribution within the fluid.

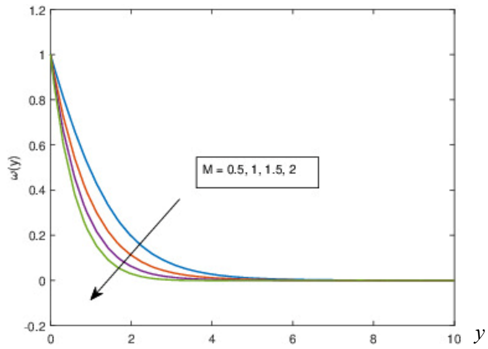

Figure 22. Role of M on ω.

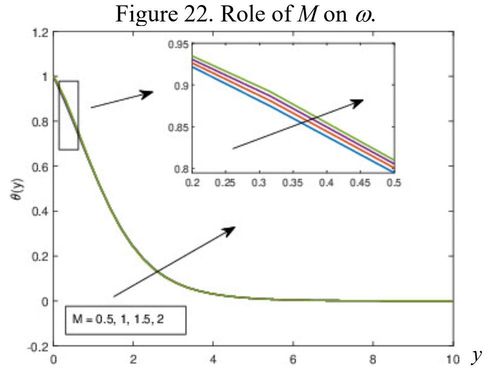

Figure 23. The role of M on θ.

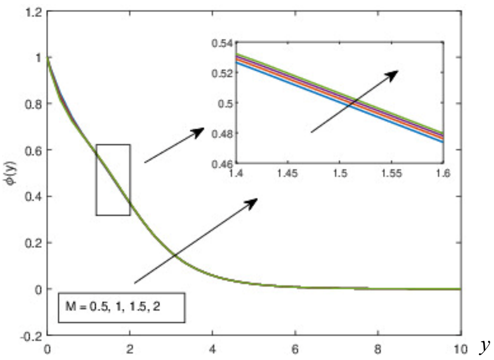

Figure 24. Role of M on ϕ.

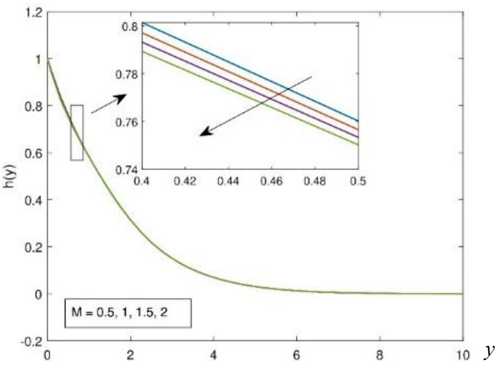

Figure 25. Role of M on h.

CONCLUSIONS

This study develops and validates the OMD-PQLM, a numerical algorithm that efficiently solves systems of nonlinear PDEs. OMD-PQLM pairs equations and solves them simultaneously while dividing the global domain into smaller overlapping subdomains. This approach achieves rapid convergence and high accuracy, requiring fewer than nine iterations to reach the stopping criterion, and the solution error decreases to the order of 10^{-14}. The method is applied to a mixed convection model of Jeffrey nanofluid motion incorporating gyrotactic microorganisms and activation energy. Residual and solution error analyses confirm its robustness. A detailed investigation of the governing parameters is performed to assess their influence. The results of the investigation show that fluid velocity decreases as the buoyancy ratios Q_1, Q_2, Prandtl number Pr, relaxation time parameter λ_1, and magnetic parameter M increase. It is also shown that microorganism density decreases with higher values of bioconvection Lewis number lb, Peclet number Pe, chemical reaction rate K, and magnetic parameter M. Conversely, the microorganism density is enhanced by a higher Prandtl number. Furthermore, the inhibition of convective transport by magnetic field results in elevated temperature and nanoparticle concentration profiles. These findings further clarify the transport phenomena within the Jeffrey nanofluid model. These overall findings indicate that OMD-PQLM provides a reliable tool for addressing complex nonlinear PDE systems in diverse scientific and engineering applications.

REFERENCES

1. Ali, F., Murtaza, S., Khan, I., et al. (2019), *Atangana-Baleanu fractional model for the flow of Jeffrey nanofluid with diffusion-thermo effects: applications in engine oil*, Adv. Differ. Equ. 2019 (1): 346. doi: 10.1186/s13662-019-2222-1
2. Hayat, T., Ali, N., Asghar, S. (2007), *An analysis of peristaltic transport for flow of a Jeffrey fluid*, Acta Mech. 193: 101-112. doi: 10.1007/s00707-007-0468-2
3. Reddy, K.V., Reddy, M.G., Makinde, O. (2019), *Thermophoresis and Brownian motion effects on magnetohydrodynamics electro-osmotic Jeffrey nanofluid peristaltic flow in asymmetric rotating microchannel*, J Nanofluids, 8(2): 349-358. doi: 10.11 66/jon.2019.1581
4. Ahmed, J., Bourazza, S., Sarfraz, M., et al. (2023), *Heat transfer in Jeffrey fluid flow over a power law lubricated surface inspired by solar radiations and magnetic flux,* Case Stud. Therm. Eng. 49: 103220. doi: 10.1016/j.csite.2023.103220
5. Tanuja, T.N., Kavitha, L., Rehman, K.U., et al. (2025), *Heat transfer in magnetohydrodynamic Jeffery-Hamel molybdenum disulfide/water hybrid nanofluid flow with thermal radiation: A neural networking analysis*, Numer. Heat Trans. Part A: Appl. 86(10): 3369-3387. doi: 10.1080/10407782.2023.2300744
6. Agarwal, V., Singh, B., Nisar, K.S. (2022), *Numerical analysis of heat transfer in magnetohydrodynamic micropolar Jeffery fluid flow through porous medium over a stretching sheet with thermal radiation*, J Therm. Anal. Calorim. 147(17): 9829-9851. doi: 10.1007/s10973-022-11224-8
7. Nadeem, S., Zaheer, S., Fang, T. (2011), *Effects of thermal radiation on the boundary layer flow of a Jeffrey fluid over an exponentially stretching surface*, Numer. Algor. 57(2): 187-205. doi: 10.1007/s11075-010-9423-8
8. Oztop, H.F., Al-Salem, K. (2012), *A review on entropy generation in natural and mixed convection heat transfer for energy systems*, Renew. Sustain. Energy Rev. 16(1): 911-920. doi: 10. 1016/j.rser.2011.09.012
9. Dong, C., Lu, G., Chen, R., et al. (2022), *Heat transfer of air turbulent mixed convection in the passive containment air-cooling system of a modular small nuclear reactor*, Int. J Therm. Sci. 182: 107793. doi: 10.1016/j.ijthermalsci.2022.107793
10. Jackson, J.D., Cotton, M.A., Axcell, B.P. (1989), *Studies of mixed convection in vertical tubes*, Int. J Heat Fluid Flow, 10 (1): 2-15. doi: 10.1016/0142-727x(89)90049-0
11. Poskas, P., Poskas, R. (2009), *Mixed convection in channel flows,* Heat Trans. Res. 40(1): 31-56. doi: 10.1615/heattransres. v40.i1.30
12. Hayat, T., Shafique, M., Tanveer, A., Alsaedi, A. (2016), *Radiative peristaltic flow of Jeffrey nanofluid with slip conditions and Joule heating*, PLoS One, 11(2): e0148002. doi: 10.1371/journ al.pone.0148002
13. Abbasi, F.M., Shehzad, S.A., Hayat, T., Alhuthali, M.S. (2016), *Mixed convection flow of Jeffrey nanofluid with thermal radiation and double stratification*, J Hydrodyn. Ser. B, 28(5): 840-849. doi: 10.1016/s1001-6058(16)60686-8
14. Saeed, M.J., Tahir, M., Asjad, M.I., et al. (2023), *Chemically radiative and mixed convection solute transfer in boundary-layer flow of Jeffrey nanofluid along an inclined stretching cylinder with Joule heating and double stratification impacts,* J Appl. Math. Mech. 103(6): e202200115. doi: 10.1002/zamm.2 02200115
15. Mohd, Z.S., Arifin, N.S., Mohd, K.A.R., Salleh, M.Z. (2020), *Suspended nanoparticles on mixed convection flow of a Jeffrey fluid due to a horizontal circular cylinder with viscous dissipation,* Therm. Sci. 24(6 Part A): 3757-3770. doi: 10.2298/tsci18 1027106m
16. Shateyi, S., Marewo, G.T. (2018), *Numerical solution of mixed convection flow of an MHD Jeffery fluid over an exponentially stretching sheet in the presence of thermal radiation and chemical reaction*, Open Phys. 16(1): 249-259. doi: 10.1515/phys-2018-0036
17. Halouani, B., Nowar, K. (2024), *Viscous dissipation and mixed convection effects on the induced magnetic field for peristaltic*

flow of a Jeffrey nanofluid, Symmetry, 16(3): 329. doi: 10.3390/sym16030329
18. Gabe, D.R. (2010), *Svante Arrhenius: discoverer of thermal activation*, Trans. IMF, 88(6): 284-284. doi: 10.1179/174591910x12869788732174
19. Ge-JiLe, H., Qayyum, S., Shah, F., et al. (2021), *Slip flow of Jeffrey nanofluid with activation energy and entropy generation applications*, Adv. Mech. Eng. 13(3): 1-9. doi: 10.1177/16878140211006578
20. Khan, N.S., Kumam, P., Thounthong, P. (2020), *Second law analysis with effects of Arrhenius activation energy and binary chemical reaction on nanofluid flow*, Sci. Rep. 10(1): 1226. doi: 10.1038/s41598-020-57802-4
21. Trivedi, M., Otegbeye, O., Ansari, M.S., Fayaz, T. (2023), *Flow of Jeffrey fluid near impulsively moving plate with nanoparticle and activation energy*, Int. J Thermofluids, 18: 100354. doi: 10.1016/j.ijft.2023.100354
22. Sarma, N., Paul, A., Patgiri, B. (2024), *Computational study of Jeffrey Hybrid nanofluid flow over on a non-uniformly heated permeable exponentially stretching surface with Arrhenius activation energy and inclined magnetic field*, Hybrid Adv. 6: 100194. doi: 10.1016/j.hybadv.2024.100194
23. Jagadesh, V., Sreenadh, S., Ajithkumar, M., et al. (2024), *Numerical exploration of the peristaltic flow of MHD Jeffrey nanofluid through a non-uniform porous channel with Arrhenius activation energy*, Numer. Heat Transf. Part A: Appl. 86(16): 5542-5556. doi: 10.1080/10407782.2024.2332477
24. Kuznetsov, A.V. (2010), *The onset of nanofluid bioconvection in a suspension containing both nanoparticles and gyrotactic microorganisms*, Int. Comm. Heat Mass Trans. 37(10): 1421-1425. doi: 10.1016/j.icheatmasstransfer.2010.08.015
25. Ansari, M.S., Otegbeye, O., Trivedi, M., Goqo, S.P. (2020), *Magnetohydrodynamic bio-convective Casson nanofluid flow: A numerical simulation by paired quasilinearisation*, J Appl. Comput. Mech. 7(4): 2024-2039. doi: 10.22055/jacm.2020.31205.1839
26. Waqas, H., Hussain, M., Alqarni, M.S., et al. (2024), *Numerical simulation for magnetic dipole in bioconvection flow of Jeffrey nanofluid with swimming motile microorganisms*, Waves Rand. Complex Media, 34(3): 1958-1975. doi: 10.1080/17455030.2021.1948634
27. Algehyne, E.A., Areshi, M., Saeed, A., et al. (2022), *Numerical simulation of bioconvective Darcy-Forchheimer nanofluid flow with energy transition over a permeable vertical plate*, Sci. Rep. 12(1): 3228. doi: 10.1038/s41598-022-07254-9
28. Alqurashi, M., Farooq, U., Sediqmal, M., et al. (2023), *Significance of melting heat in bioconvection flow of micropolar nanofluid over an oscillating surface*, Sci. Rep. 13(1): 11692. doi: 10.1038/s41598-023-38361-w
29. Alzahrani, J., Aziz, S., Hamoudi, M.R., et al. (2023), *Evaluation of bioconvection for sinusoidally moving Jeffrey nanoparticles in view of temperature dependent thermal conductivity and Cattaneo-Christov heat diffusion model*, Ain Shams Eng. J, 14(9): 102124. doi: 10.1016/j.asej.2023.102124
30. Garg, A., Sharma, Y.D., Jain, S.K. (2023), *Stability analysis of thermo-bioconvection flow of Jeffrey fluid containing gravitactic microorganism into an anisotropic porous medium*, Forces Mech. 10: 100152. doi: 10.1016/j.finmec.2022.100152
31. Ali, Z., Imran, M., Tahir, M., et al. (2024), *Numerical investigation of bioconvective non-Newtonian nanofluid flow across a curved surface in the presence of microbes*, Case Stud. Therm. Eng. 64: 105308. doi: 10.1016/j.csite.2024.105308
32. Ahsan, N., Khan, M.N., Alqurashi, M.S., et al. (2024), *Bioconvective magnetized flow analysis of a tangent hyperbolic nanofluid with nonuniform source/sink over an exponentially porous stretching sheet*, J Appl. Math. Mech. 104(12): e202300966. doi: 10.1002/zamm.202300966
33. Canuto, C., Hussaini, M.Y., Quarteroni, A., Zang, T.A., Spectral Methods in Fluid Dynamics, Springer-Verlag, Berlin, 1988. doi: 10.1007/978-3-642-84108-8
34. Pasban, A., Sadrnia, H., Mohebbi, M., Shahidi, S.A. (2017), *Spectral method for simulating 3d heat and mass transfer during drying of apple slices*, J Food Eng. 212: 201-212. doi: 10.1016/j.jfoodeng.2017.05.013
35. Oloniiju, S.D., Mukwevho, N., Tijani, Y.O., Otegbeye, O. (2024), *Chebyshev pseudospectral method for fractional differential equations in non-overlapping partitioned domains*, Appl. Math, 4(3): 950-974. doi: 10.3390/appliedmath4030051
36. Acharya, N. (2020), *Spectral quasi linearization simulation of radiative nanofluidic transport over a bended surface considering the effects of multiple convective conditions*, Eur. J Mech. - B/Fluids, 84: 139-154. doi: 10.1016/j.euromechflu.2020.06.004
37. Motsa, S.S. (2013), *A new spectral local linearization method for nonlinear boundary layer flow problems*, J Appl. Math. 2013 (1): 423628. doi: 10.1155/2013/423628
38. Motsa, S.S., Dlamini, P.G., Khumalo, M. (2014), *Spectral relaxation method and spectral quasilinearization method for solving unsteady boundary layer flow problems*, Adv. Math. Phys. 2014(1): 341964. doi: 10.1155/2014/341964
39. Otegbeye, O., *On paired decoupled quasi-linearization methods for solving nonlinear systems of differential equations that model boundary layer fluid flow problems*, PhD Thesis, University of KwaZulu-Natal, Pietermaritzburg, 2018.
40. Otegbeye, O., Goqo, S.P., Ansari, M.S. (2020), *Comparative study of some spectral based methods for solving boundary layer flow problems*, AIP Conf. Proc. 2253(1): 020013. doi: 10.1063/5.0019230
41. Magagula, V.M., Motsa, S.S., Sibanda, P. (2020), *Multidomain bivariate pseudo-spectral quasilinearization method for systems of nonlinear partial differential equations*, Comput. Math. Methods, 2(4): e1096. doi: 10.1002/cmm4.1096
42. Mathale, D., *A multi-domain implementation of the pseudo-spectral method and compact finite difference schemes for solving time-dependent differential equations*, MSc Thesis, University of Johannesburg, South Africa, 2019.
43. Mkhatshwa, M., Motsa, S., Sibanda, P. (2021), *Overlapping multi-domain bivariate spectral method for systems of nonlinear PDEs with fluid mechanics applications*, In: Rushi Kumar, B., Sivaraj, R., Prakash, J. (Eds.) Advances in Fluid Dynamics. Lecture Notes in Mechanical Engineering. Springer, Singapore, pp.685-699. doi: 10.1007/978-981-15-4308-1_54
44. Nefale, M.M., Ayano, M.S., Otegbeye, O., Oloniiju, S.D. (2025), *Overlapping multi-domain paired quasilinearization method for the solution of the MHD Williamson-nanofluid flow over an exponentially stretching surface*, J Adv. Res. Fluid Mech. Therm. Sci. 126(1): 17-38. doi: 10.37934/arfmts.126.1.1738
45. Khan, S.U., Tlili, I. (2020), *Significance of activation energy and effective Prandtl number in accelerated flow of Jeffrey nanoparticles with gyrotactic microorganisms*, J Energy Resour. Technol. 142(11): 112101. doi: 10.1115/1.4047248
46. Trefethen, L.N., Spectral Methods in MATLAB, SIAM, 2000. doi: 10.1137/1.9780898719598